# *Ab Initio* Lifetime and Concomitant Double-Excitation Character of Plasmons at Metallic Densities

Alan M. Lewis[1] and Timothy C. Berkelbach[2,3,*]
[1]*Department of Chemistry and James Franck Institute, University of Chicago, Chicago, Illinois 60637, USA*
[2]*Department of Chemistry, Columbia University, New York, New York 10027 USA*
[3]*Center for Computational Quantum Physics, Flatiron Institute, New York, New York 10010, USA*

(Received 15 October 2018; published 7 June 2019)

The accurate calculation of excited state properties of interacting electrons in the condensed phase is an immense challenge in computational physics. Here, we use state-of-the-art equation-of-motion coupled-cluster theory with single and double excitations (EOM-CCSD) to calculate the dynamic structure factor, which can be experimentally measured by inelastic x-ray and electron scattering. Our calculations are performed on the uniform electron gas at densities corresponding to Wigner-Seitz radii of $r_s = 5$, 4, and 3 corresponding to the valence electron densities of common metals. We compare our results to those obtained using the random-phase approximation (RPA), which is known to provide a reasonable description of the collective plasmon excitation and which resums only a small subset of the polarizability diagrams included in EOM-CCSD. We find that EOM-CCSD, instead of providing a perturbative improvement on the RPA plasmon, predicts a many-state plasmon resonance, where each contributing state has a double-excitation character of 80% or more. This finding amounts to an *ab initio* treatment of the plasmon linewidth, which is in good quantitative agreement with previous diagrammatic calculations, and highlights the strongly correlated nature of lifetime effects in condensed-phase electronic structure theory.

DOI: 10.1103/PhysRevLett.122.226402

*Introduction.*—The uniform electron gas (UEG) is a paradigmatic model of interacting electrons in the condensed phase [1,2]. Finite-order perturbation theory for the ground-state correlation energy exhibits a divergence due to the UEG's metallic character and long-ranged Coulomb interactions. These divergences are famously removed by the infinite-order resummation of time-independent particle-hole ring diagrams known as the random-phase approximation (RPA) [3,4]. As a dynamical theory of the density response function, the RPA corresponds to a resummation of all time-dependent ring diagrams and forms the microscopic basis for screening the Coulomb interaction, as is done, for example, in the *GW* approximation [5]. In the UEG, the RPA strongly modifies the noninteracting polarizability, most significantly predicting the existence of a collective plasmon excitation. Outside of the particle-hole continuum, the RPA plasmon is a coherent, dispersive excitation with infinite lifetime; inside the particle-hole continuum, it acquires a lifetime due to Landau damping.

A number of calculations have attempted to improve on the RPA treatment of the UEG density response function, in order to uncover signatures of electron correlation and to test new theoretical tools. Previous works extend the RPA through the selective inclusion of a static or dynamic local field correction [6–12], which is closely related to time-dependent density functional theory. However, fully *ab initio* nonperturbative techniques are now reaching a point of maturity where they can be applied in an unbiased manner to large, condensed-phase systems. Here, we use equation-of-motion coupled-cluster theory with single and double excitations (EOM-CCSD) [13–17] to calculate the density response function of the UEG and to compare to that predicted by the RPA. As shown previously [18,19], EOM-CCSD rigorously resums a larger class of time-dependent diagrams than those included in the RPA. In particular, beyond the RPA ring diagrams, the EOM-CCSD response function includes all ladder diagrams, mixed ring-ladder diagrams, and exchange diagrams, as well as large classes of diagrams associated with two particle-hole pairs (i.e., double excitations in the excited-state wave function). The CC formalism is appropriate for periodic systems because it has total energies that are size extensive [16]. Recent years have seen intense activity on the applications of perturbation theory, RPA, and CC theory to realistic materials, with encouraging results [20–28]. However, excited-state CC techniques [13,17] have been studied significantly less in the solid state, despite their attractive properties. For example, unlike quantum Monte Carlo approaches, EOM-CCSD directly constructs spectral functions on the real frequency axis, and does not require analytic continuation. To the best of our knowledge, this work represents the first calculation of neutral excitation spectra of a periodic, condensed-phase system using EOM-CCSD. This technological advance opens the door for highly accurate simulations of excitonic and plasmonic phenomena in atomistic materials.

 © 2019 American Physical Society

*Theory.*—Our calculations are performed in a finite simulation cell with periodic boundary conditions in the canonical ensemble at zero temperature. The simulation cell contains $N$ electrons in a volume $\Omega = L^3$. The electron density is $n = N/\Omega$ and the Wigner-Seitz radius, measuring the average size of a sphere occupied by one electron, is $r_s = [3/(4\pi n)]^{1/3}$. The pairwise Coulomb interaction is treated with the periodic Ewald interaction [29–31] assuming a compensating background charge. The one-electron basis functions are plane waves, $\psi_{\boldsymbol{k}}(\boldsymbol{r}) = \Omega^{-1/2}\exp(i\boldsymbol{k}\cdot\boldsymbol{r})$ where $\boldsymbol{k} = (2\pi/L)[l, m, n]$ and $l$, $m$, $n$ are integers. For closed-shell electron configurations, the spectrum of the finite UEG is always gapped but becomes increasingly metallic at large system sizes. In the correlated calculations to follow, we use $N = 66$ electrons in a single-particle basis of 81 plane-wave orbitals, corresponding to a density-dependent kinetic energy cutoff. This system size is comparable to those used in ground-state quantum Monte Carlo [32–37] and quantum chemistry [38–44] calculations on the UEG, for which finite-size and basis set effects have been studied more methodically. The computational cost of these CCSD calculations scales like $N^2M^4$. For these parameters, the ground-state CCSD calculation, which is only performed once for each value of $r_s$, is relatively cheap. Although EOM-CCSD has the same formal scaling, the calculation of the dynamic structure factor is our bottleneck, because of the many frequency points and challenges associated with the solution of a system of linear equations. We have performed simple finite-size analysis and believe that our conclusions remain valid in the thermodynamic limit.

Our primary observable is the dynamic structure factor $S(\boldsymbol{q},\omega) = -\pi^{-1}\mathrm{Im}\Pi(\boldsymbol{q},\omega)$, where $\Pi(\boldsymbol{q},\omega)$ is the polarizability, i.e., the Fourier transform of the retarded density response function,

$$\Pi(\boldsymbol{q},\omega) = -i\int_0^\infty dt e^{i\omega t}\langle\Psi_0|[\rho(\boldsymbol{q},t),\rho^\dagger(\boldsymbol{q},0)]|\Psi_0\rangle, \tag{1}$$

with $\rho^\dagger(\boldsymbol{q}) = \sum_{\boldsymbol{k}} a^\dagger_{\boldsymbol{k}+\boldsymbol{q}}a_{\boldsymbol{k}}$. For the noninteracting electron gas, the polarizability can be simply computed, $\Pi^0(\boldsymbol{q},\omega) = \sum_{\boldsymbol{k}}[n_{\boldsymbol{k}} - n_{\boldsymbol{k}+\boldsymbol{q}}]/[\hbar\omega - (\varepsilon_{\boldsymbol{k}+\boldsymbol{q}} - \varepsilon_{\boldsymbol{k}}) + i\eta]$. The noninteracting structure factor has a particle-hole continuum with boundaries determined by the Fermi occupancy functions $n_{\boldsymbol{k}}$. The exact polarizability can be formally given by

$$\Pi(\boldsymbol{q},\omega) = \frac{\Pi^0(\boldsymbol{q},\omega)}{1 - v(q)[1 - G(\boldsymbol{q},\omega)]\Pi^0(\boldsymbol{q},\omega)}, \tag{2}$$

where $G(\boldsymbol{q},\omega)$ is a dynamic local field factor. The RPA polarizability, which resums all time-dependent ring diagrams, is obtained for $G(\boldsymbol{q},\omega) = 0$ and exhibits a pole associated with the collective, plasmon excitation. As long as the plasmon energy falls outside of the particle-hole continuum, the RPA predicts it to have an infinite lifetime; in other words, even in the thermodynamic limit, the RPA plasmon is a *single quantum state*. Inside the particle-hole continuum, the plasmon interacts with quasiparticle excitations, leading to Landau damping and a finite lifetime. In the long-wavelength limit, the RPA is exact [2] and the plasmon dispersion approaches the classical plasma energy $\omega_{\mathrm{P}}(q \to 0) = \sqrt{4\pi n}$. At finite $q$, the exact plasmon dispersion is unknown; however, by analyzing the limiting behaviors and conservation laws, one can argue that the exact plasmon dispersion lies below that predicted by the RPA [2]. Therefore, an exact treatment of the UEG is expected to produce a plasmon with a displacement to lower energies and with a finite lifetime, both due to interaction with multipair excitations beyond the RPA.

In recent work, one of us (T. C. B.) showed that the polarizability diagrams summed in the RPA are a strict subset of those included in the EOM-CCSD polarizability [18]. However, because our analysis will make use of the EOM-CCSD excited-state wave functions, we briefly review the plasmon wave function implied by the RPA and by the simpler Tamm-Dancoff approximation (TDA) [45]. In the TDA, we consider all allowed single-excitation, one-particle+one-hole ($1p1h$) states, $|\Psi_{\mathrm{TDA}}(\boldsymbol{q})\rangle = \sum'_{\boldsymbol{k}} r^{\boldsymbol{k}+\boldsymbol{q}}_{\boldsymbol{k}} a^\dagger_{\boldsymbol{k}+\boldsymbol{q}}a_{\boldsymbol{k}}|0\rangle$, where here and throughout the primed summation enforces that $\boldsymbol{k}$ is an occupied state and $\boldsymbol{k}+\boldsymbol{q}$ is an unoccupied state in the mean-field reference $|0\rangle$. Neglecting electron-hole exchange and solving the configuration interaction problem leads to the identification of the plasmon wave function

$$|\Psi^{\mathrm{P}}_{\mathrm{TDA}}(\boldsymbol{q})\rangle = N(q)\sum_{\boldsymbol{k}}{}' \frac{1}{\omega_{\mathrm{TDA}}(q) - (\varepsilon_{\boldsymbol{k}+\boldsymbol{q}} - \varepsilon_{\boldsymbol{k}})} a^\dagger_{\boldsymbol{k}+\boldsymbol{q}}a_{\boldsymbol{k}}|0\rangle, \tag{3}$$

where $N(q)$ is a normalization factor. The TDA plasmon energy $\omega_{\mathrm{TDA}}(q)$ is the largest root of the secular equation,

$$1 = v(q)\sum_{\boldsymbol{k}}{}' \frac{1}{\omega_{\mathrm{TDA}}(q) - (\varepsilon_{\boldsymbol{k}+\boldsymbol{q}} - \varepsilon_{\boldsymbol{k}})}, \tag{4}$$

where $v(q) = 4\pi/q^2$. The TDA plasmon wave function is a coherent superposition of all allowed $1p1h$ excitations, with equal positive weights in the $q \to 0$ limit, $N'\rho_{\boldsymbol{q}}|0\rangle$. Though physically transparent, the TDA yields a plasmon energy with an unphysical divergence as $q \to 0$. This behavior is fixed in the RPA, which resums ring diagrams in both the forward and backward time directions. The backward propagations are consistent with correlation in the ground-state wave function. Following the recent result of Ref. [18], the RPA wave functions can be written as a coherent superposition of single excitations on a correlated ground-state wave function $|\Psi_0\rangle = e^{T_2}|0\rangle$,

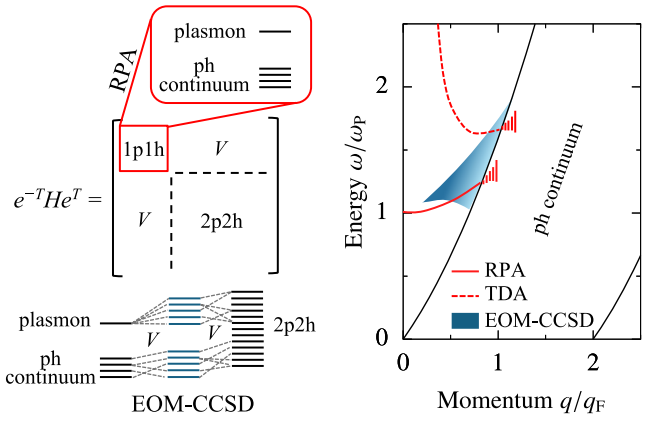


FIG. 1. Schematic of the main methods and results of the this work. EOM-CCSD diagonalizes a similarity-transformed Hamiltonian in the $1p1h$ and $2p2h$ configuration space; diagonalization within the $1p1h$ space gives the RPA result (plus minor corrections [18]), which yields a collective plasmon split off from the remaining ph continuum. The interaction of these states with $2p2h$ configurations produces new eigenstates, as shown in the bottom left. The single plasmon state is mixed into many eigenstates, giving it an effective lifetime, although each individual eigenstate has predominantly $2p2h$ character. As shown at the right, this leads to a plasmon dispersion that is slightly higher than that of the RPA, in contrast to the known exact behavior, but with a proper correlation-induced lifetime.

$$|\Psi_{\mathrm{RPA}}(\boldsymbol{q})\rangle = \sum_{k}^{\prime} r_{k}^{k+q} a_{k+q}^{\dagger} a_{k} e^{T_2}|0\rangle, \tag{5}$$

where $T_2 = \sum_{k_1 k_2 q}^{\prime} t_{k_1,k_2}^{q} a_{k_1+q}^{\dagger} a_{k_2-q}^{\dagger} a_{k_2} a_{k_1}$ is a double-excitation operator with amplitudes $t_{k_1,k_2}^{q}$ satisfying the ring-CCD (RPA) equations [18,46,47]. It is simple to show that the RPA plasmon amplitudes $r_{k}^{k+q}$ have the same form as those of the TDA,

$$|\Psi_{\mathrm{RPA}}^{\mathrm{P}}(\boldsymbol{q})\rangle = N(q) \sum_{k}^{\prime} \frac{1}{\omega_{\mathrm{RPA}}(q) - (\varepsilon_{k+q} - \varepsilon_{k})} a_{k+q}^{\dagger} a_{k} e^{T_2}|0\rangle \tag{6}$$

but with the improved RPA plasmon dispersion $\omega_{\mathrm{RPA}}(q)$. Therefore, we conclude that the RPA plasmon wave function is characterized by a constructive superposition of single excitations on a CCD ground state.

Electronic states with *dominant single-excitation character* are known to be improved by the inclusion of double excitations corresponding to two-particle+two-hole ($2p2h$) configurations. In periodic EOM-CCSD, the excited-state wave functions are given by

$$\begin{aligned}|\Psi_{\mathrm{CC}}(\boldsymbol{q})\rangle &= \Bigg(\sum_{k}^{\prime} r_{k}^{k+q} a_{k+q}^{\dagger} a_{k} \\ &\quad + \sum_{k_1,k_2,k_3}^{\prime} r_{k_1,k_2}^{k_3,k_1+k_2-k_3+q} a_{k_3}^{\dagger} a_{k_1+k_2-k_3+q}^{\dagger} a_{k_2} a_{k_1}\Bigg) e^{T_2}|0\rangle,\end{aligned} \tag{7}$$

and thus include both single and double excitations with respect to the correlated ground-state wave function ($T_2$ is obtained from the full CCSD equations and $T_1$ is zero for the UEG). Therefore, EOM-CCSD is expected to provide an improved description of the plasmon, whose entire theoretical description to date has relied upon a single-excitation picture. This formalism is equivalent to the diagonalization of the similarity-transformed Hamiltonian matrix in the basis of $1p1h$ and $2p2h$ configurations, as shown in Fig. 1.

Detailed expressions for the RPA, TDA, and EOM-CCSD polarizability are given in the Supplemental Material [48].

*Results.*—In Fig. 2, we show the dynamic structure factor at $r_s = 4$ calculated using the noninteracting theory in

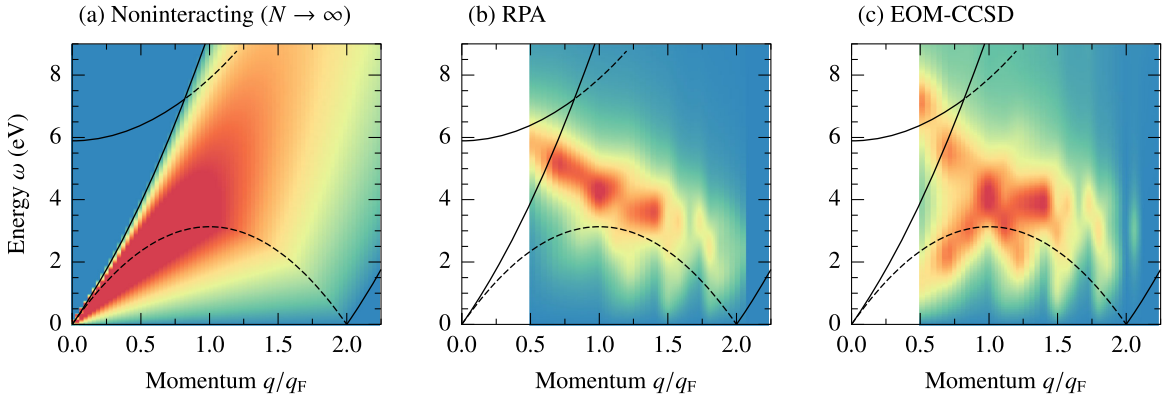


FIG. 2. Dynamic structure factor of the uniform electron gas at $r_s = 4$ obtained in the thermodynamic limit for the noninteracting theory (a) and for the finite system from the RPA (b) and EOM-CCSD theory (c). Finite-sized calculations have $N = 66$ electrons with $M = 81$ plane-wave basis functions. Solid and dashed black lines indicate the boundaries and maximum intensity of independent-particle excitations and the dispersion of the plasmon calculated in the RPA. A broadening of $\eta = 1$ eV is used in the RPA and EOM-CCSD calculations.

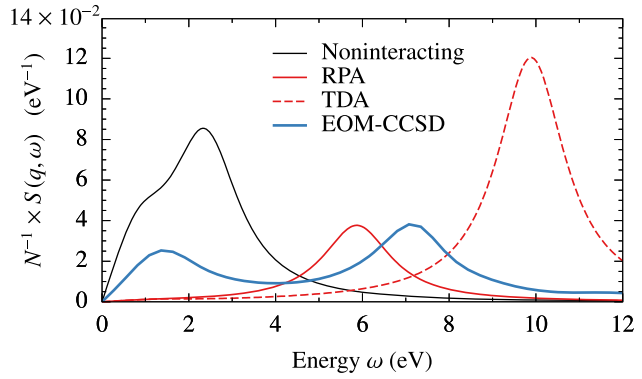


FIG. 3. Dynamic structure factor of the UEG at $r_s = 4$ with $N = 66$ electrons in $M = 81$ plane-wave basis functions at $q \approx q_F/2$. A broadening of $\eta = 1$ eV is used in all calculations.

the thermodynamic limit (a) as well as the RPA (b) and EOM-CCSD (c) results for $N = 66$ electrons with $M = 81$ plane-wave basis functions. Ignoring symmetries, the EOM-CCSD Hamiltonian includes more than $2 \times 10^6$ many-body states. Because of the finite system size, in all calculations we use a broadening of $\eta = 1$ eV. The simulation data are unavailable at large $q$ because of the finite basis set and at small $q$ because of the finite system size. In particular, for an $N$-electron simulation, the smallest accessible value of the momentum transfer is $q = 2\pi/L \approx 2.03 q_F/N^{1/3}$, where $q_F$ is the Fermi wave vector; for $N = 66$ electrons, this corresponds to $q \approx q_F/2$. In the Supplemental Material [48], we present a thorough study of finite basis effects and finite size effects at the RPA level, for which large calculations are affordable; we confirm that the properties studied here are not strongly affected.

Despite the finite system size, the plasmon peak at $q = q_F/2$ is separated from the particle-hole continuum and can be confidently assigned and analyzed. In Fig. 3, we show the dynamic structure factor at $q = q_F/2$ calculated using various theories for the 66-electron system. The correlated theories are consistent with expected behavior, showing a redistribution of oscillator strength from the particle-hole continuum into the plasmon resonance. Interestingly, the EOM-CCSD spectrum maintains a non-negligible intensity in the low-energy region, which can also be seen in Fig. 2(c). The energies of the RPA and TDA plasmons are close to their values in the thermodynamic limit. However, contrary to expectations, the EOM-CCSD plasmon is located at a *higher* energy than the RPA plasmon, in disagreement with the known exact behavior.

To understand this behavior, we analyze the wave function character of the states contributing to the plasmon peak. Unlike the TDA or RPA, for which the plasmon peak comes from a *single* quantum state, EOM-CCSD predicts a plasmon peak that is composed of many states; i.e., it has a physical linewidth due to interactions with multipair configurations. This correlation-induced linewidth is masked by

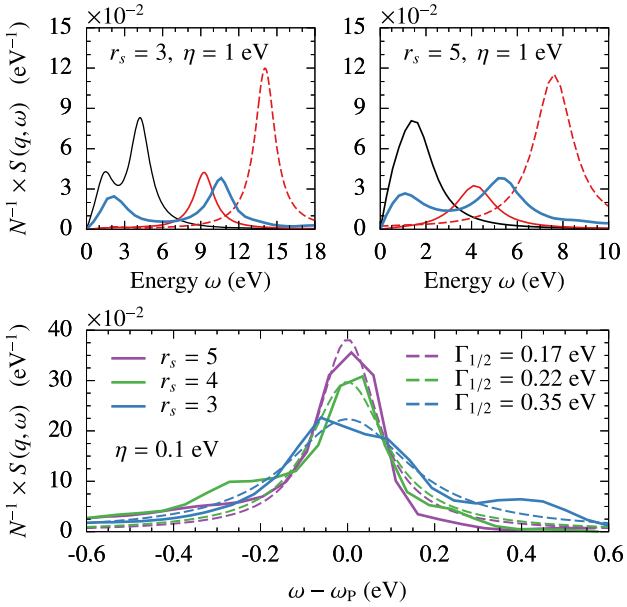


FIG. 4. The same as in Fig. 3, but for $r_s = 3$ (top left) and $r_s = 5$ (top right). At higher densities (smaller $r_s$), the plasmon peak at $q = q_F/2$ is much closer to the particle-hole continuum, leading to the enhanced broadening of the EOM-CCSD plasmon, which can be resolved with a smaller numerical broadening of $\eta = 0.1$ eV (bottom). Dashed lines demonstrate a Lorentzian fit where $\Gamma_{1/2}$ is the half-width at the half-maximum.

the use of the relatively large line broadening factor $\eta = 1$ eV. To characterize these states, we use an energy-targeting algorithm that locates interior eigenvalues of the EOM-CCSD Hamiltonian. Remarkably, we find that *all* states contributing to the plasmon peak have a significant double-excitation (two-partice, two-hole) character; the state that contributes most strongly to the plasmon peak has only 17% single-excitation character and 83% double-excitation character. This result is in apparent contrast to the usual picture of the plasmon as a single quantum state that is well described as being dominated by single excitations but is consistent with a many-body lifetime of such a single quantum state. The wave function character of the contributing many-body states also explains the incorrect behavior of the plasmon dispersion: EOM-CCSD is known to overestimate the excitation energy of states with significant double-excitation character. A quantitative prediction of the plasmon energy would require the use of triple excitations (three-particle, three-hole configurations) to allow orbital relaxation in the presence of double excitations.

To test these conclusions, we calculated the dynamic structure factor at higher and lower densities. In Fig. 4, we show the dynamic structure factors calculated at $q = q_F/2$, for $r_s = 3$ and $r_s = 5$. Consistent with our findings at $r_s = 4$, we see that the EOM-CCSD plasmon is situated in between those of the RPA and TDA, but with a broad line shape and background due to strong mixing with multipair excitations. At higher density (smaller $r_s$), the importance

of the Coulomb interaction is reduced, the RPA is more accurate, and the wave functions are less strongly correlated. Also, the plasmon is shifted to higher energies. However, the plasmon at the minimum value of $q$ accessible in our 66-electron simulation becomes closer to the particle-hole continuum and lifetime effects are expected to increase. At a given value of $q/q_{\mathrm{F}}$, the linewidth is roughly proportional to the plasmon energy [49], and thus we expect to see an increased plasmon linewidth for decreasing $r_s$, despite the decrease in electron correlation. As mentioned above, the physical linewidth is masked by the use of a relatively large broadening $\eta = 1$ eV, which was chosen to minimize finite-size effects in the particle-hole continuum. In order to estimate the interaction-induced linewidth, we recalculated the dynamic structure factor near the plasmon peak using a much smaller broadening $\eta = 0.1$ eV, shown in the bottom panel of Fig. 4. With decreasing $r_s$, the plasmon peak acquires significant spectral structure indicative of contributions from multiple many-electron states. By fitting to a Lorentzian line shape, we extract an approximate plasmon linewidth, which is found to be $\Gamma_{1/2} = 0.17, 0.22, 0.35$ eV for $r_s = 5, 4, 3$. We emphasize that the RPA linewidth is precisely the numerical broadening $\Gamma_{1/2} = \eta = 0.1$ eV for all values for $r_s$ at this momentum.

Previous diagrammatic calculations on the electron gas have made predictions of the plasmon linewidth [49–52]. At leading order in $q$, the plasmon linewidth at our studied value of $q = q_{\mathrm{F}}/2$ is given by $\Gamma_{1/2} = b\omega_{\mathrm{P}}/4$, where $b$ is calculated by the theory. The results of Ref. [49] are based on a pair factorization of the four-particle Green's function, $G_4 \approx G_2 G_2$. When the noninteracting $G_2$ is used in the factorization, $b$ is on the order of unity; when the RPA-screened $G_2$ is used in the factorization, $b$ is significantly reduced to 0.1 or less [49]. Using $b = 0.1$ predicts a linewidth of $\Gamma_{1/2} = 0.10, 0.15, 0.23$ eV for $r_s = 5, 4, 3$, in surprisingly good quantitative agreement with our EOM-CCSD results. We note that the polarizability diagrams responsible for lifetime effects in EOM-CCSD go beyond the factorization approximation and include interactions between particle-hole pairs [18], although the screening of such interactions does not include all time-orderings included in the RPA [53].

*Conclusions.*—We have demonstrated that EOM-CCSD is a promising method for the study of electronic spectra in condensed-phase systems. Most significantly, the inclusion of double excitations in EOM-CCSD enables the *ab initio* calculation of interaction-induced lifetimes of quasiparticle resonances. Here, the wave-function-based nature of EOM-CCSD allowed a precise characterization of the many-body quantum states contributing to the plasmon resonance, which were found to have significant double-excitation character.

The low single-excitation character of the states contributing to the plasmon resonance is consistent with the characterization of the plasmon as a quasiparticle excitation; i.e., the quasiparticle weight of the entire plasmon resonance is conserved, but necessarily shared by the many quantum states contributing. This observation has important implications for *ab initio* calculations of condensed-phase spectra: the hybridization responsible for non-negligible electronic linewidths directly implies a large double-excitation character, which may lead to an overestimation of excitation energies. This may be responsible for the slight overestimation of the energy of the plasmon satellite peaks observed in a previous application of EOM-CCSD to the one-particle spectral function of the UEG [27]. Future work in this direction should pursue the use of triple excitations in order to realize an *ab initio* method capable of predicting accurate energies and lifetimes of condensed-phase quasiparticle excitations. Comparison to other post-RPA methods, such as the real-time Kadanoff-Baym approach [54] or the Bethe-Salpeter equation [55] would also be interesting. Additionally, studies at larger system sizes and in larger basis sets will allow the investigation of the modified plasmon dispersion inside the particle-hole continuum as well as the asymmetry and fine structure of the dynamic structure factor [56].

The multipair nature of the plasmon uncovered here also has a number of experimental implications, despite the fact that phonons and interband scattering can obscure the plasmon's correlation-induced lifetime [52,57]. In one direction, the physics described here is potentially important for cold-atom experiments, which provide isolation from a thermalizing environment and access to electronic relaxation processes [58]. Additionally, we expect that the physics described here can be observed in nanomaterials, such as graphene plasmonics [59] or zero-dimensional quantum dots. In these latter examples, a phonon bottleneck may inhibit phonon emission [60], leading plasmons and excitons to decay into multipair excitations, i.e., an inverse Auger effect. This phenomenon is at the heart of multiple exciton generation [61] and singlet exciton fission [62].

All calculations were performed with the PySCF software package [63], using resources provided by the University of Chicago Research Computing Center. This work was supported by the Air Force Office of Scientific Research under Award No. FA9550-18-1-0058. Research at the Flatiron Institute is supported by the Simons Foundation.

*tim.berkelbach@gmail.com

[1] D. Pines and P. Nozieres, *The Theory of Quantum Liquids: Volume 1* (CRC Press, London, 1994).
[2] G. Giuliani and G. Vignale, *Quantum Theory of the Electron Liquid* (Cambridge University Press, Cambridge, England, 2008).
[3] D. Bohm and D. Pines, Phys. Rev. **92**, 609 (1953).

[4] M. Gell-Mann and K. A. Brueckner, Phys. Rev. **106**, 364 (1957).
[5] L. Hedin, Phys. Rev. **139**, A796 (1965).
[6] K. S. Singwi, M. P. Tosi, R. H. Land, and A. Sjolander, Phys. Rev. **176**, 589 (1968).
[7] K. S. Singwi, A. Sjolander, M. P. Tosi, and R. H. Land, Phys. Rev. B **1**, 1044 (1970).
[8] P. Vashishta and K. S. Singwi, Phys. Rev. B **6**, 875 (1972).
[9] A. A. Kugler, J. Stat. Phys. **12**, 35 (1975).
[10] G. Mukhopadhyay, R. K. Kalia, and K. S. Singwi, Phys. Rev. Lett. **34**, 950 (1975).
[11] B. Dabrowski, Phys. Rev. B **34**, 4989 (1986).
[12] Z. Qian and G. Vignale, Phys. Rev. B **65**, 235121 (2002).
[13] H. Koch and P. Jorgensen, J. Chem. Phys. **93**, 3333 (1990).
[14] J. F. Stanton and R. J. Bartlett, J. Chem. Phys. **98**, 7029 (1993).
[15] R. Kobayashi, H. Koch, and P. Jorgensen, Chem. Phys. Lett. **219**, 30 (1994).
[16] R. J. Bartlett and M. Musiał, Rev. Mod. Phys. **79**, 291 (2007).
[17] A. I. Krylov, Annu. Rev. Phys. Chem. **59**, 433 (2008).
[18] T. C. Berkelbach, J. Chem. Phys. **149**, 041103 (2018).
[19] K. Emrich, Nucl. Phys. **A351**, 397 (1981).
[20] L. Schimka, J. Harl, A. Stroppa, A. Grüneis, M. Marsman, F. Mittendorfer, and G. Kresse, Nat. Mater. **9**, 741 (2010).
[21] T. Olsen, J. Yan, J. J. Mortensen, and K. S. Thygesen, Phys. Rev. Lett. **107**, 156401 (2011).
[22] J. Paier, X. Ren, P. Rinke, G. E. Scuseria, A. Grüneis, G. Kresse, and M. Scheffler, New J. Phys. **14**, 043002 (2012).
[23] G. Booth, A. Grüneis, G. Kresse, and A. Alavi, Nature (London) **493**, 365 (2013).
[24] J. J. Shepherd and A. Grüneis, Phys. Rev. Lett. **110**, 226401 (2013).
[25] A. Grüneis, G. Kresse, Y. Hinuma, and F. Oba, Phys. Rev. Lett. **112**, 096401 (2014).
[26] A. Grüneis, Phys. Rev. Lett. **115**, 066402 (2015).
[27] J. McClain, J. Lischner, T. Watson, D. A. Matthews, E. Ronca, S. G. Louie, T. C. Berkelbach, and G. K.-L. Chan, Phys. Rev. B **93**, 235139 (2016).
[28] T. Gruber, K. Liao, T. Tsatsoulis, F. Hummel, and A. Grüneis, Phys. Rev. X **8**, 021043 (2018).
[29] L. M. Fraser, W. M. C. Foulkes, G. Rajagopal, R. J. Needs, S. D. Kenny, and A. J. Williamson, Phys. Rev. B **53**, 1814 (1996).
[30] S. Chiesa, D. M. Ceperley, R. M. Martin, and M. Holzmann, Phys. Rev. Lett. **97**, 076404 (2006).
[31] N. D. Drummond, R. J. Needs, A. Sorouri, and W. M. C. Foulkes, Phys. Rev. B **78**, 125106 (2008).
[32] D. M. Ceperley and B. J. Alder, Phys. Rev. Lett. **45**, 566 (1980).
[33] S. Moroni, D. M. Ceperley, and G. Senatore, Phys. Rev. Lett. **75**, 689 (1995).
[34] Y. Kwon, D. M. Ceperley, and R. M. Martin, Phys. Rev. B **58**, 6800 (1998).
[35] H. Kwee, S. Zhang, and H. Krakauer, Phys. Rev. Lett. **100**, 126404 (2008).
[36] N. D. Drummond and R. J. Needs, Phys. Rev. Lett. **102**, 126402 (2009).
[37] T. Dornheim, S. Groth, T. Schoof, C. Hann, and M. Bonitz, Phys. Rev. B **93**, 205134 (2016).
[38] J. J. Shepherd, G. Booth, A. Grüneis, and A. Alavi, Phys. Rev. B **85**, 081103 (2012).
[39] J. J. Shepherd, A. Grüneis, G. H. Booth, G. Kresse, and A. Alavi, Phys. Rev. B **86**, 035111 (2012).
[40] A. Gruneis, J. J. Shepherd, A. Alavi, D. P. Tew, and G. H. Booth, J. Chem. Phys. **139**, 084112 (2013).
[41] J. J. Shepherd, T. M. Henderson, and G. E. Scuseria, J. Chem. Phys. **140**, 124102 (2014).
[42] J. J. Shepherd, T. M. Henderson, and G. E. Scuseria, Phys. Rev. Lett. **112**, 133002 (2014).
[43] J. J. Shepherd, J. Chem. Phys. **145**, 031104 (2016).
[44] J. S. Spencer and A. J. Thom, J. Chem. Phys. **144**, 084108 (2016).
[45] P. Ring and P. Shuck, *The Nuclear Many-Body Problem* (Springer-Verlag, Berlin Heidelberg, 1980).
[46] D. L. Freeman, Phys. Rev. B **15**, 5512 (1977).
[47] G. E. Scuseria, T. M. Henderson, and D. C. Sorensen, J. Chem. Phys. **129**, 231101 (2008).
[48] See Supplemental Material at http://link.aps.org/supplemental/10.1103/PhysRevLett.122.226402 for detailed RPA and CCSD expressions and for finite-size and finite-basis studies at the RPA level.
[49] M. Hasegawa and M. Watabe, J. Phys. Soc. Jpn. **27**, 1393 (1969).
[50] D. DuBois, Ann. Phys. (N.Y.) **8**, 24 (1959).
[51] B. W. Ninham, C. J. Powell, and N. Swanson, Phys. Rev. **145**, 209 (1966).
[52] D. F. Dubois and M. G. Kivelson, Phys. Rev. **186**, 409 (1969).
[53] M. F. Lange and T. C. Berkelbach, J. Chem. Theory Comput. **14**, 4224 (2018).
[54] N. H. Kwong and M. Bonitz, Phys. Rev. Lett. **84**, 1768 (2000).
[55] E. Maggio and G. Kresse, Phys. Rev. B **93**, 235113 (2016).
[56] S. Ichimaru, Rev. Mod. Phys. **54**, 1017 (1982).
[57] W. Ku and A. G. Eguiluz, Phys. Rev. Lett. **82**, 2350 (1999).
[58] M. Gring, M. Kuhnert, T. Langen, T. Kitagawa, B. Rauer, M. Schreitl, I. Mazets, D. A. Smith, E. Demler, and J. Schmiedmayer, Science **337**, 1318 (2012).
[59] H. Yan, T. Low, W. Zhu, Y. Wu, M. Freitag, X. Li, F. Guinea, P. Avouris, and F. Xia, Nat. Photonics **7**, 394 (2013).
[60] J. Urayama, T. B. Norris, J. Singh, and P. Bhattacharya, Phys. Rev. Lett. **86**, 4930 (2001).
[61] A. J. Nozik, Chem. Phys. Lett. **457**, 3 (2008).
[62] K. Miyata, F. S. Conrad-Burton, F. L. Geyer, and X. Y. Zhu, Chem. Rev. **119**, 4261 (2019).
[63] Q. Sun, T. C. Berkelbach, N. S. Blunt, G. H. Booth, S. Guo, Z. Li, J. Liu, J. D. McClain, E. R. Sayfutyarova, S. Sharma, S. Wouters, and G. K. L. Chan, Comput. Mol. Sci. **8**, e1340 (2018).